Edición a cargo de: Violeta Ramos Radilla y Javier Lara Espinosa

PUBLICADO POR EL CENTRO NACIONAL DE PREVENCION DE DESASTRES DE LA SECRETARIA DE GOBERNACION

Distribución en México: Coordinación de Enlace Nacional
Distribución en el Exterior: Coordinación de Asuntos Internacionales

Julio - 1994, No. 15

Sistema Nacional de Protección Civil

SISTEMA NACIONAL DE PROTECCION CIVIL

CENTRO NACIONAL DE PREVENCION DE DESASTRES

A STUDY ON NONLINEAR FINITE ELEMENT ANALYSIS OF CONFINED MASONRY WALLS

Kazuhiko Ishibashi
Hideo Kastumata

COORDINACION DE INVESTIGACION

AREA DE ENSAYES SISMICOS

CUADERNOS DE INVESTIGACION

P R E S E N T A C I O N

La Coordinación de Investigación del Centro Nacional de Prevención de Desastres realiza estudios sobre las características de los fenómenos naturales y de las actividades humanas que son fuentes potenciales de desastres, así como sobre las técnicas y medidas que conducen a la reducción de las consecuencias de dichos fenómenos.

Las actividades enfocan la problemática de los Riesgos Geológicos (Sismos y Volcanes), de los Riesgos Hidrometeorológicos (Inundaciones, Huracanes, Sequías, Erosión) y de los Riesgos Químicos (Incendios, Explosiones, Contaminación por Desechos Industriales).

Los resultados de los estudios se publican en Informes Técnicos que se distribuyen a las instituciones y los especialistas relacionados con cada tema específico.

En adición a dichos informes técnicos de carácter muy especializado, el CENAPRED ha emprendido la publicación de esta serie, llamada CUADERNOS DE INVESTIGACION, con el fin de dar a conocer a un público más amplio aquellos estudios que se consideran de interés más general o que contienen información que conviene quede publicada en una edición más formal que la de los Informes Técnicos.

Los Catálogos de Informes Técnicos y de Cuadernos de Investigación, así como las publicaciones específicas pueden obtenerse solicitándolos por escrito a la Coordinación de Investigación del CENAPRED, o pueden consultarse directamente en su Unidad de Información.

A Study of Nonlinear Finite Element Analysis of Confined Masonry Walls

by

Kazuhiko Ishibashi and Hideo Katsumata

1. INTRODUCTION

A series of experiments was carried out from 1991 to 1992 at CENAPRED in order to investigate the behavior of confined masonry structure systems (brick masonry load-bearing walls confined by light reinforced concrete bond-beams and tie-columns) subjected to horizontal loads[1),2)] Five types of confined masonry structures were tested, providing much information on failure modes, load-deflection relations, hysteretic behavior, etc., which are very valuable for understanding their seismic behavior.

In order to obtain more general information on the seismic behavior of confined masonry structures, development of theoretical methods for analysis is essential. The major problem in developing such methods lies on the difficulty of modeling the mechanical characteristics of joints between bricks and the confinement reinforced concrete beams or columns in masonry walls. This is because the nature of joints is that of a mechanical discontinuity.

The finite element method, at this time, is the most suitable tool for analyzing the behavior of structures which have mechanical discontinuities. The authors have tried to develop an appropriate finite element model suitable for analyzing the seismic behavior of confined masonry structures. For this purpose, results of the experiments mentioned above have been utilized. In the Appendix of this paper, results of the first stage in the development, which is related to the modeling of boundary surfaces between masonry walls and surrounding reinforced concrete elements are described. In the present paper, related to the second phase, results of the application of the finite element method to the five tests of the experiments are presented.

The computer program used for analyses in this study is the code named "FINAL", which was developed at the Technical Research Institute of Obayashi Corporation, Japan. This program has been applied to static nonlinear finite element analyses for reinforced concrete structures and in the program the nonlinearity of material characteristics can be considered.

2. LOADING CONDITIONS SUPPOSED

In the experiments, test specimens were subjected to reversed cyclic horizontal loads. In the analysis, with one exception to be stated below, one-way monotonic incremental loads were supposed, because at this time both the behavior of confined masonry structures under reversed cyclic loading, and the phenomena that cracks in walls or concrete may open very widely under reversed cyclic loading cannot be simulated.

Brick masonry walls of the test specimen WBW-B in the experiments were reinforced with horizontal high-strength deformed wires against horizontal shear force and, therefore, cracks in the brick walls were suppressed from developing so widely (see Section 3). In the analysis of this specimen only, one cycle of reversed loading was supposed in the range of small horizontal displacements.

3. ANALYTICAL MODELING OF TEST SPECIMENS

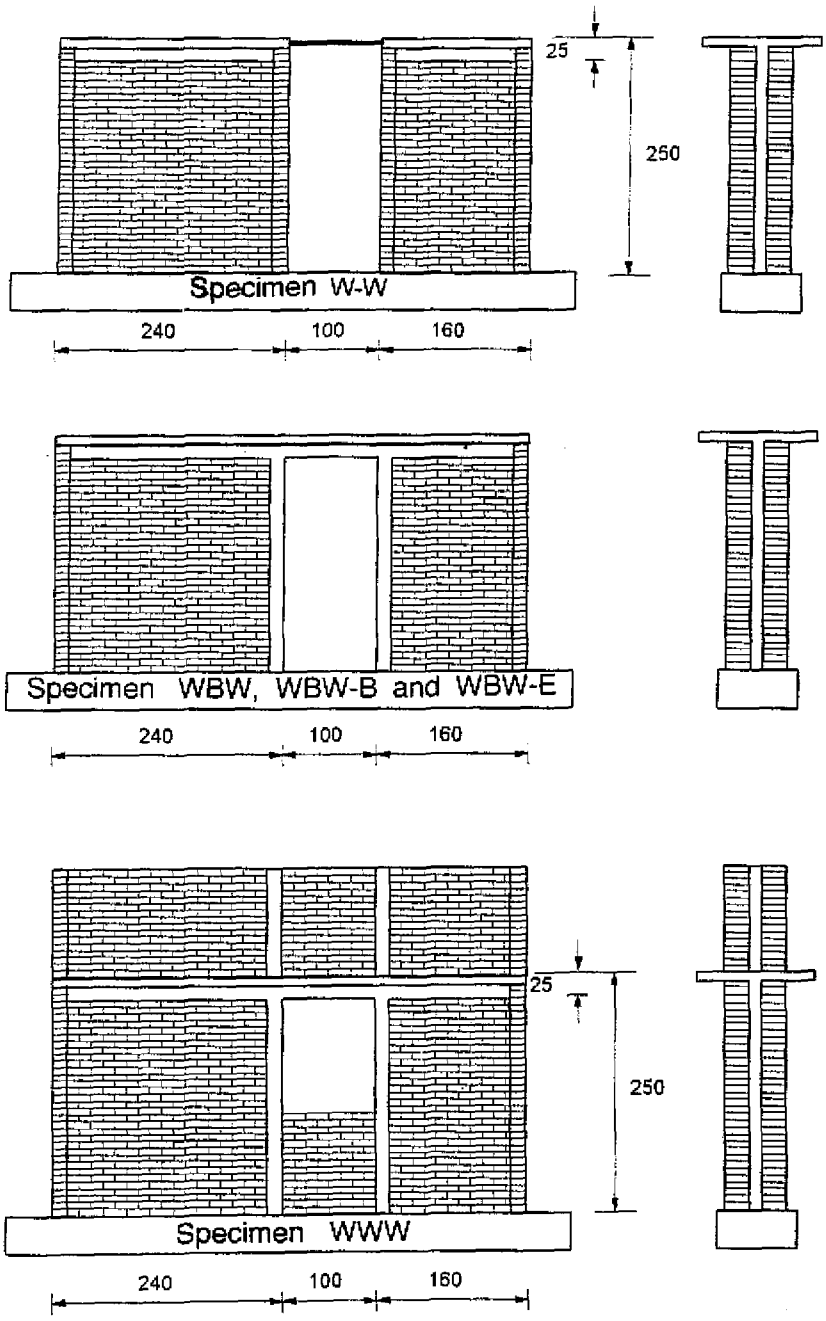

Fig. 3.1 Geometry of test specimens (units in cm)

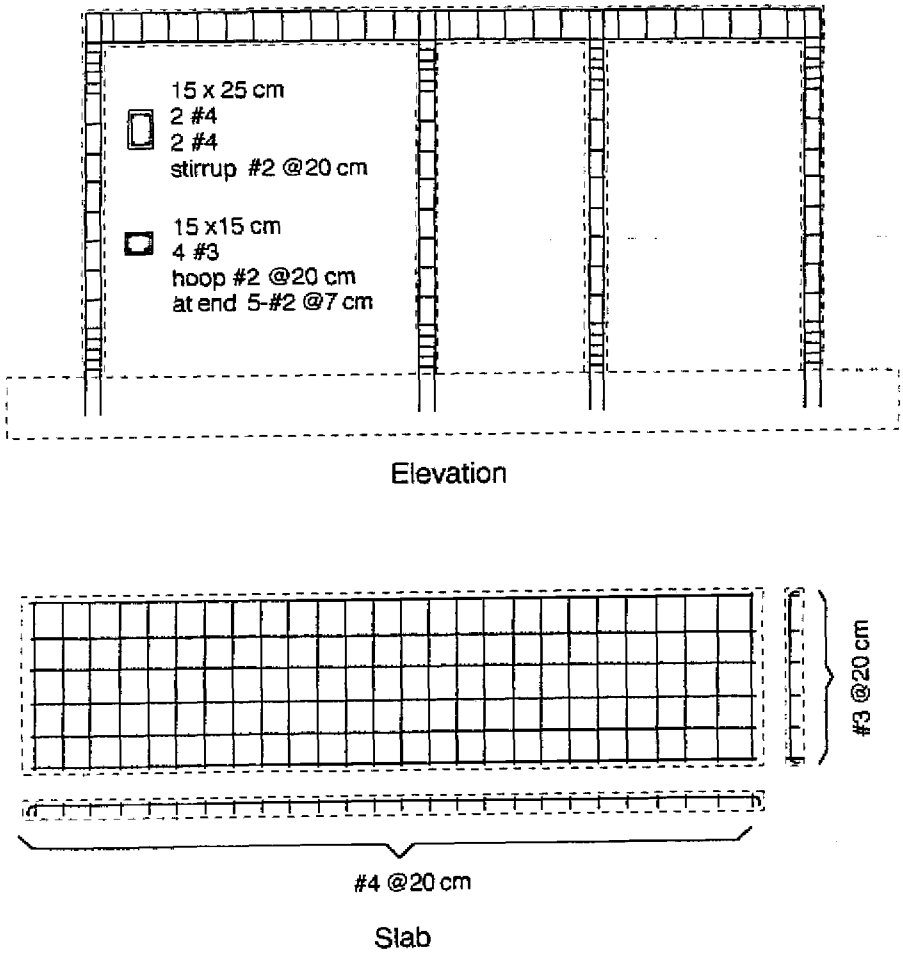

Fig. 3.2 Reinforcement for confinement reinforced concrete elements and slabs of test specimens

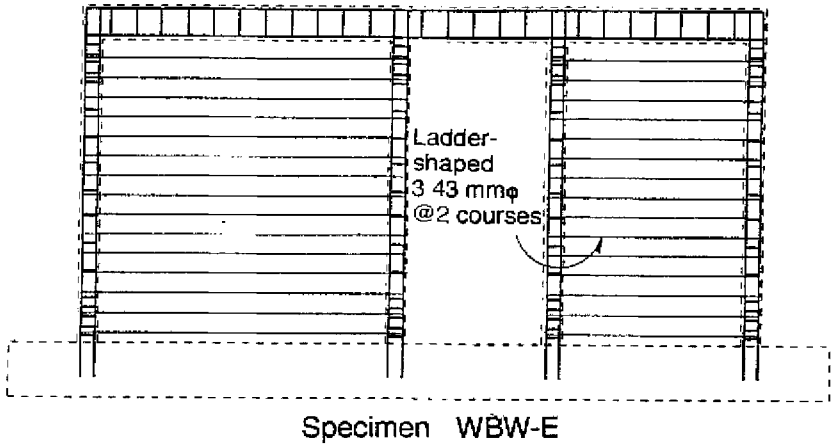

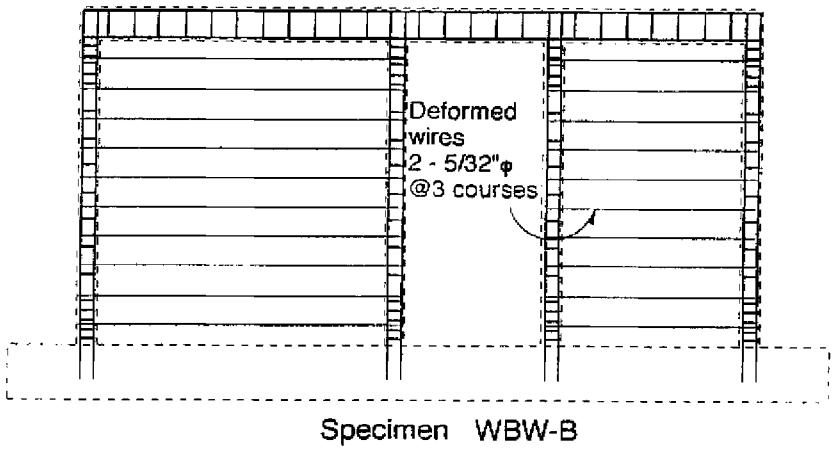

Fig. 3.3 Reinforcement for brick masonry walls for test specimens WBW-E and WBW-B. Brick masonry walls of specimens W-W, WBW and WWW were not reinforced.

3.1 Description of Test Specimens

Geometry and re-bar arrangements of the five test specimens used in the Experiments are shown in Figs 3.1 to 3.3. Specimens were different by the type of connection between the two walls, the existence of parapet walls and the amount and type of horizontal shear reinforcement in brick walls as follows;

Specimen WBW	:	Two walls were connected by a beam and a slab. Brick walls were not reinforced. Hereinafter, it is called as prototype specimen.
Specimen W-W	:	Two walls were connected with steel rods.
Specimen WWW	:	Parapet walls were added to the prototype specimen.
Specimen WBW-E	:	Brick walls of the prototype specimen were reinforced with ladder-shaped high-strength horizontal reinforcement at every two courses with a nominal reinforcement ratio of 0.089%.
Specimen WBW-B	:	Brick walls of the prototype specimen were reinforced with horizontal high-strength deformed wires at every three courses with a nominal reinforcement ratio of 0.089%.

The loading system used in the experiments is shown in Fig. 3.4.

3.2 Modeling of Test Specimen

In this analysis, the following assumptions were postulated for modeling the test specimens;

1) The plane stress condition was assumed in the analyses.
2) Effects of the foundation slab on the behavior of specimens would be negligible, so all the specimens were supposed to be completely fixed at the top of the foundation beam.
3) Four-node quadrilateral plane stress elements were used for modeling brick walls.
4) A tie-column and two buttress walls which had been connected to the tie-beam were supposed to be one element having the superimposed characteristics of a reinforced concrete element and a brick wall element.

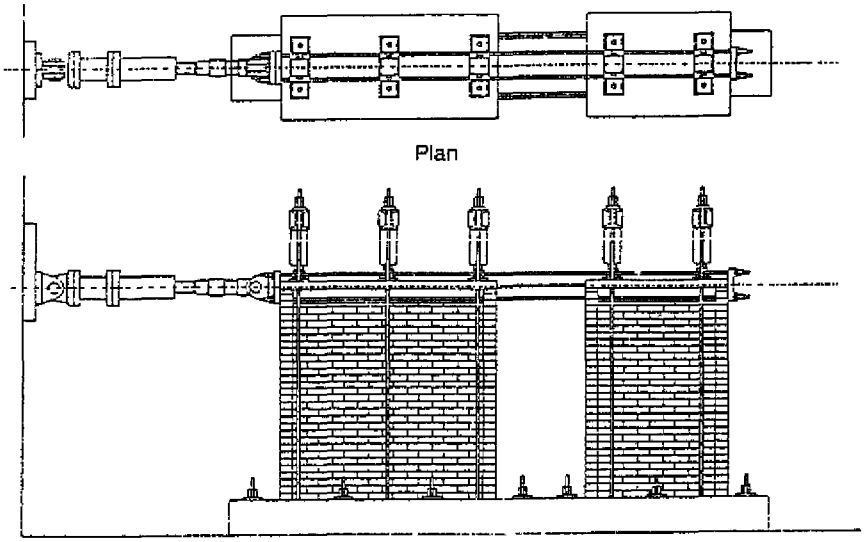

Fig. 3.4 Loading system

5) Steel rods of specimen W-W were replaced by a truss element.

6) In Figs 3.5 to 3.7 the finite element mesh supposed and the location of loading points are indicated. Each quadrilateral finite element for brick walls has the same characteristics as those obtained in masonry prisms. This was adopted to decrease the number of finite elements. The element height is supposed to be approximately equal to two courses. The horizontal size of the elements is selected to be approximately equal to the height. Size of quadrilateral finite elements was the same for all specimens.

7) Longitudinal and shear reinforcement in peripheral reinforced concrete elements were replaced with elements having tensile stiffness in one direction and those elements were superimposed on the plane stress elements for columns or beams.

8) Horizontal reinforcement in brick walls was replaced by truss elements.

9) Tensile strength of horizontal joint mortar in brick walls was about three times larger than that of bricks. So, horizontal joints were replaced with equivalent spring elements each having two nodes. Each spring was located between the upper nodes of a lower brick finite element and the lower nodes of an upper brick finite element.

10) In the experiments, with increasing horizontal loads, separation and slippage were observed along the boundary surface between brick walls and peripheral reinforced concrete tie-columns. In order to simulate this phenomenon, brick wall elements and elements for peripheral bond-beams and tie-columns were connected by a two-node linkage element consisting of a pair of orthogonal springs.

11) External forces in the vertical direction were divided into three components and were applied to nearest three nodes to the loading points of the experiments. Horizontal loads were divided in two concentrated forces and were applied to the two nodes shown in Figs 3.5 to 3.7.

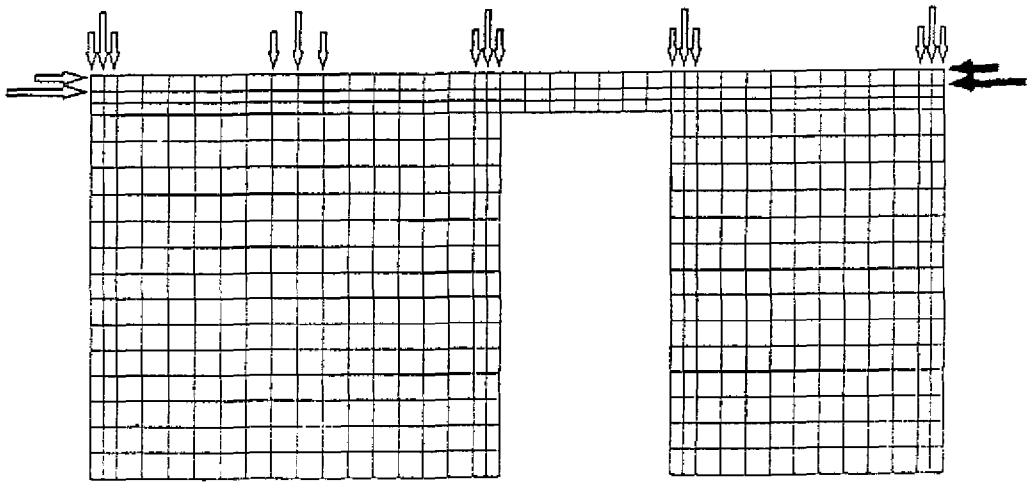

Fig. 3.5 Finite element mesh and loading points for Specimens WBW, WBW-E and WBW-B

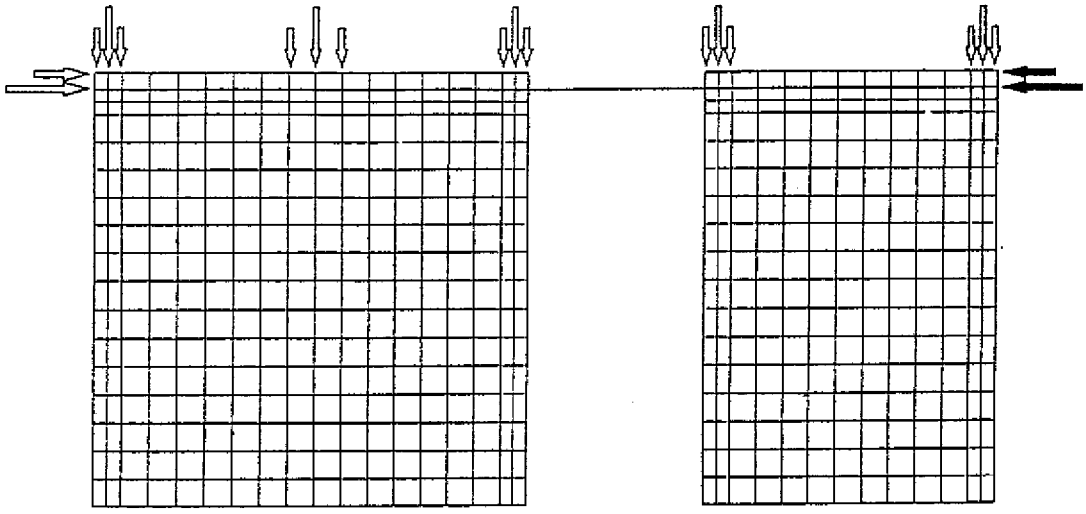

Fig. 3.6 Finite element mesh and loading points for Specimen W-W

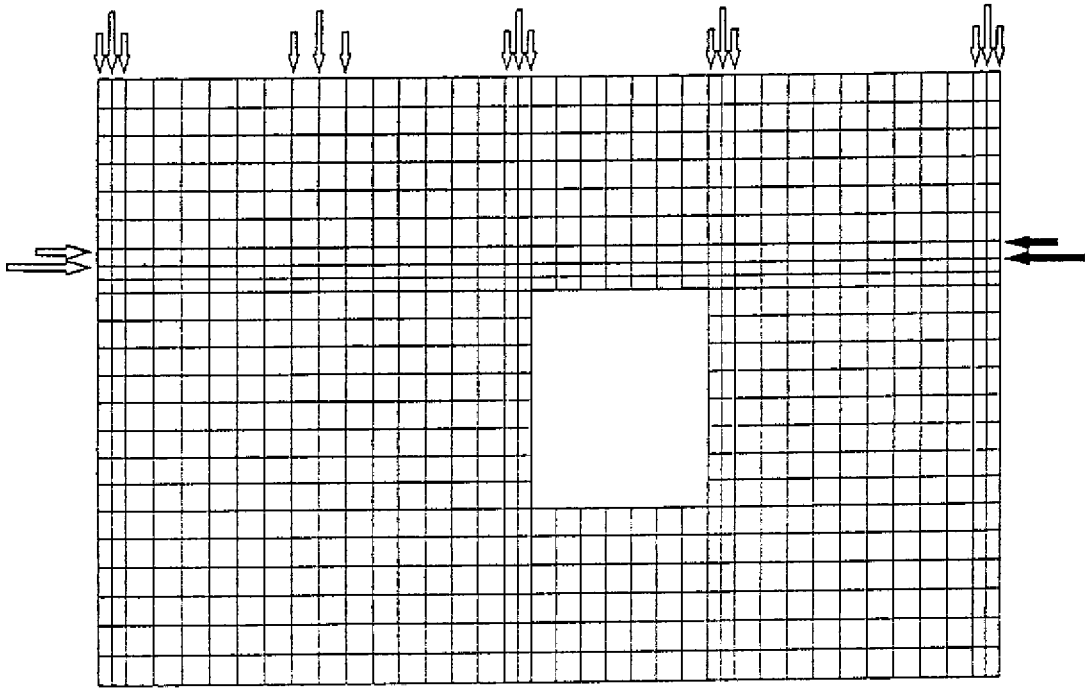

Fig. 3.7 Finite element mesh and loading points for Specimen WWW

4. ANALYTICAL MODELING OF MATERIAL CHARACTERISTICS

Material characteristics were supposed as follows:

1) Mechanical characteristics of masonry prisms, concrete, joint mortar and re-bars were those results of material tests conducted in the experiments.

2) Constitutive law of concrete under the plane-stress condition followed the orthotropic model proposed by Darwin *et al.*[3] under the concept of equivalent uniaxial strain.

3) Failure criteria of concrete under biaxial stress condition followed the equation proposed by Kupfer *et al.*[4].

4) The stress-strain relationship of concrete was supposed as shown in Fig. 4.1: linear-elastic up to the occurrence of cracking in tension, and nonlinear as expressed by the exponential function proposed by Fafitis *et al.*[5] for compression.

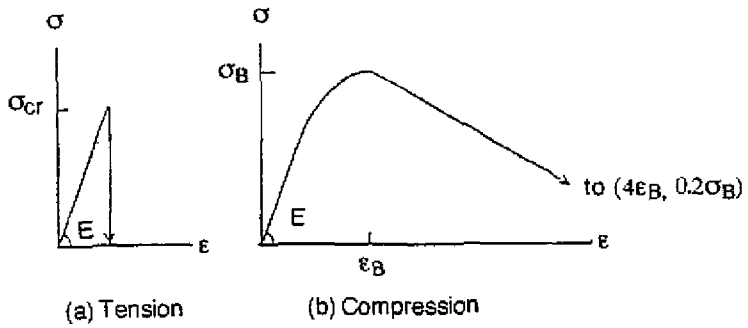

Fig. 4.1 Stress (σ)-strain (ϵ) relationship for concrete, where E: Young's modulus, σ_{cr}: uniaxial tensile strength, σ_B: uniaxial compressive strength and ϵ_B: strain at peak stress σ_B.

5) Cracking in concrete was judged to occur depending on the magnitude of principal stress. After cracking, the stress and stiffness in the direction normal to the crack were assumed equal to zero.

6) Assumptions 2) to 5) were also applied to masonry prisms.

7) The stress-strain relationship of steel reinforcement in peripheral confinement elements was supposed to be bilinear as shown in Fig. 4.2 (a). Stiffness after yielding was assumed as 1/100 of Young's modulus.

8) The yield point of walls' horizontal reinforcement was not well-defined; the stress-strain curve was typical of high-strength cold formed bars. Therefore, the trilinear stress-strain relationship shown in Fig. 4.2 (b) was assumed.

9) Material constants for concrete and bars used in the analyses are listed in Tables 4.1 and 4.2. From the measured Young's modulus, the tensile strength of concrete and strain at the compressive strength were derived from empirical formulae as a function of uniaxial compressive strength. As for the Poisson's ratio, a conventional value of 0.167 was assumed.

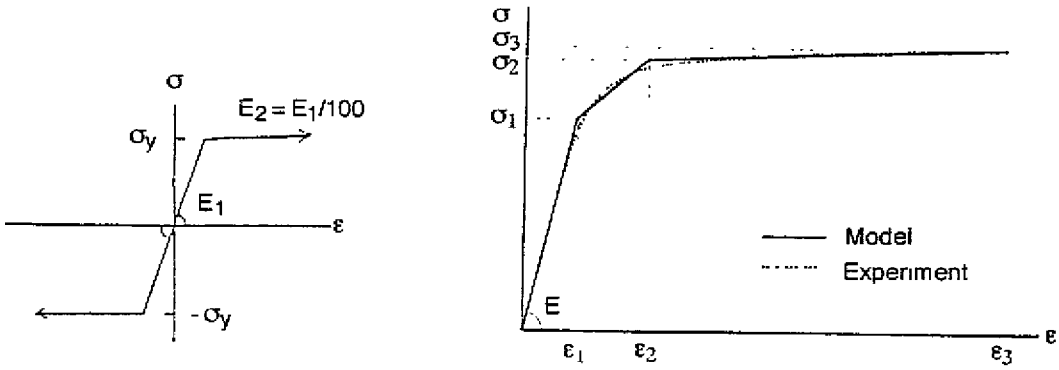

Fig. 4.2 Stress (σ)-strain (ϵ) relationship for bars used in the confinement frame (left) and as horizontal reinforcement in brick masonry walls (right), where E_1 and E are Young's modulus and σ_y is yield stress. Values of E, σ_1 to σ_3 and ϵ_1 to ϵ_3 assumed in the calculation are listed in Table 4.1.

Table 4.1 Material constants assumed in the calculation (see Fig. 4.2)

	E	σ_1	σ_2	σ_3	ϵ_1	ϵ_2	ϵ_3
WBW-E	1.86	5000	6000	6600	2688	5000	20000
WBW-B	1.97	6000	7190	7470	3046	5916	20000
Unit	10^6 kgf/cm^2	kgf/cm^2			micro-strain		

Table 4.2 Material constants of concrete

Test Specimen		E*1 (10^5 kgf/cm^2)	ν*2	σ_B*3 (kgf/cm^2)	ϵ_B*4 (micro-strain)	σ_t*5 (kgf/cm^2)
WBW	Column	2.04	0.167	164.5	1915	19.2
	Beam/Slab	2.73		356.5	2178	29 8
W-W	Column	2 31		228.5	2003	23.1
	Beam/Slab	3 10		489 2	2360	35.6
WWW	Column	1.89		132.5	1872	17.0
	Beam/Slab	2.74		358.2	2181	29.9
WBW-E	Column	2.27		220.0	1991	22.7
	Beam/Slab	2.50		284.0	2079	26.2
WBW-B	Column	2.26		217.0	1987	22.5
	Beam/Slab	2.36		242.0	2022	23 9

*1: Young's modulus calculated from eq $E = 0\ 114 \cdot \sqrt{\sigma_B + 0.582}$ (after Ref.8)
*2: Poisson's ratio
*3: Uniaxial compressive strength; results of material tests from the experiments
*4: Strain at uniaxial strength calculated from $\epsilon_B = (1.37\sigma_B + 1690) \times 10^6$ (after Ref.8)
*5: Uniaxial tensile strength calculated from $\sigma_t = 1.07\sigma_B^{0.566}$ (after Ref.9)

Table 4 3 Material constants of reinforcing bars

Reinforcing bars	Cross Sectional Area (cm^2)	Young's Modulus E (10^6 kgf/cm^2)	Yield Strength σ_y (kgf/cm^2)
Longitudinal bar #4 for WBW-B	1.27	1 98	4450
for others	1.27	1 92	4220
Longitudinal bar #3 for WBW-B	0.71	2.01	4510
for others	0.71	1 88	4630
Shear bars #2 for WBW-B	0.32	1 97	2810
for others	0.32	2 01	2750
Horizontal reinforcement #1 for WBW-E	0.08	1 86	6040
for WBW-B	0.12	1 97	7190

10) Material constants for masonry prisms used in the analysis are listed in Table 4.4. Young's modulus was calculated according to the formula proposed in the Mexico City Building Code[6]. Compressive strengths in the table are values obtained from compression tests in the experiments. The tensile strength of masonry prism was assumed to be equal to 1/10 of its compressive strength based on flexural tests of bricks. Poisson's ratio for masonry prism was supposed equal to that of concrete

11) Characteristics of the linkage element located in the boundary between the masonry panel and the RC confining elements were assumed as follows:

i) The spring constant for stresses normal to boundary surfaces was 1.0×10^8 kgf/cm and the normal stress-displacement relation was the one shown in Fig. 4.3 (a),

ii) The shear stress-shear slip relation in the direction parallel to the boundary surface was that shown in Fig. 4.3 (b), where the effect of normal compressive stress acting on the surface was based on the results of shear tests on brick joints carried out by Fujii *et al.*[7]. Here, the shear stress τ_u at the turning point is

$$\tau_u = \tau_l + 0.8\sigma_n \qquad [1]$$

where τ_l is 20% of the shear strength obtained from diagonal compression tests of masonry walls (see footnote[1]) and σ_n is the normal compressive stress acting on the boundary surface. From Eq. [1], the friction coefficient between masonry prisms and the surrounding RC elements was supposed to be 0.8.

In case that the normal stress σ_n is tensile, σ_n in Eq. [1] and stiffness K_2 in Fig. 4.3 (b) is assumed to be zero.

---

[1] At the time when the shear slip occurs under diagonal compression, shear stress τ_u is equal to normal stress σ_n:

$$\tau_u = \sigma_n \qquad [f1]$$

Supposing the friction coefficient is 0.8, we can get the following equation:

$$\tau_u = \tau_l + 0.8\sigma_n \qquad [f2]$$

Substituting Eq [f1] for Eq [f2], we get

$$\tau_l = 0.2\tau_u$$

12) The spring elements which represent the characteristics of joint mortar between bricks were assumed to have load-displacement characteristics as shown in Fig. 4.4

Table 4.4 Material constants for masonry prisms

	E*1 (kgf/cm²)	ν*2	σ_B*3 (kgf/cm²)	ϵ_B*4	σ_t*5 (kgf/cm²)
WBW	3.237 x 10^4	0.167	53.95	0.002	5.395
W-W	2.980 x 10^4		49.67		4.967
WWW	3.024 x 10^4		50.40		5 040
WBW-E	2.895 x 10^4		48.25		4.825
WBW-B	2.991 x 10^4		49.85		4.985

*1: Young's modulus calculated from $E=600\sigma_B$ (after Ref 6)
*2: Poisson's ratio
*3: Uniaxial compressive strength; results of material tests in the experiments
*4: Strain at uniaxial compressive strength estimated from $\sigma_B/E=0.001667$
*5: Uniaxial tensile strength calculated from $\sigma_t=\sigma_B/10$

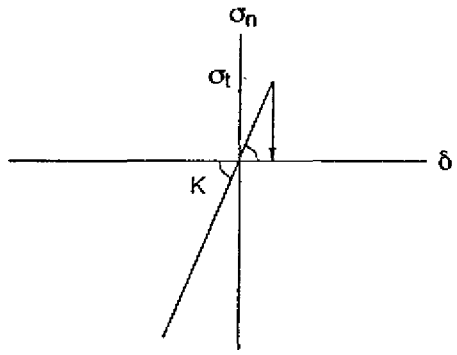

Fig. 4.3 (a) Normal stress (σ_n)-displacement (δ) relationship at the boundary between brick masonry walls and peripheral reinforced concrete frames, where K = 1.0 x 10^8 kg/cm and σ_t is the tensile strength of bricks.

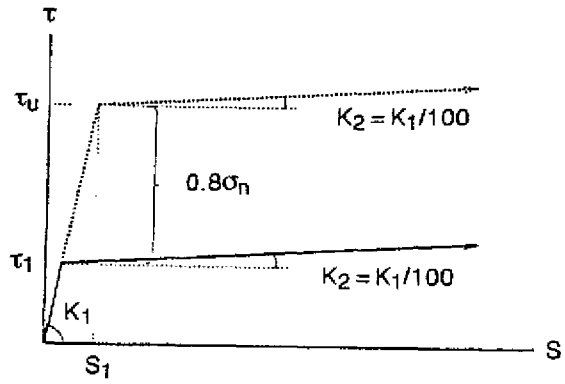

Fig. 4.3 (b) Shear stress (τ)-shear slip (S) relationship at the boundary between brick masonry walls and peripheral reinforced concrete frames, where τ_u = 9.2 kgf/cm^2, τ_1 = 1.84 kgf/cm^2 and S_1 = 0.1 mm.

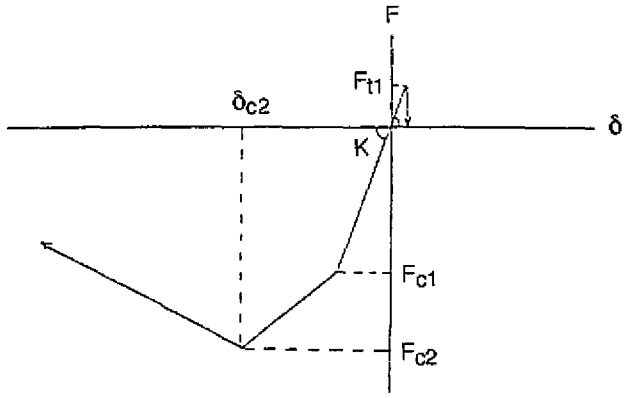

Fig. 4.4 Load (F)-displacement (δ) characteristics for spring elements at horizontal joints, where values for K, F_{t1}, F_{c2} and δ_{c2} correspond to Young's modulus of joint mortar (4 x 10^5 kgf/cm^2), tensile strength of joint mortar (560 kgf), compressive strength of joint mortar (4629 kgf) and displacement calculated from the strain of joint mortar (0.028 cm) at the compressive strength, respectively. F_{c1} was supposed to be 60% of F_{c2}.

5. CONDITION SETTING FOR ANALYSIS

Nineteen sets of conditions were prepared for calculation as listed on Table 5.1. Horizontal and vertical loading conditions were major factors to produce those variations. The other factor was the pretension in the steel rods, which were used to connect the top of the two walls of test specimen W-W. In the experiments, 6 t of pretension in total were recorded in the rods before starting the horizontal loading. The aim of Case 7 in the table is to

examine the effects of this pretension, so that where 6 t of pretension were introduced into the connecting rods before starting horizontal loading and were maintained up to the final stage of calculation.

In Table 5.1, "positive" or "negative" direction of horizontal loading corresponds to the cases that the horizontal load is applied to the top of walls "from left to right" or "from right to left" on Fig. 3.1, respectively. A vertical load of 25 t was applied to test specimens. A vertical load of 30 t and 20 t are equal to a 20% increase and decrease from 25 t, respectively

Cases 18 and 19 correspond to a positive and negative loading cycle of a reversed one-cycle of loading, respectively

Table 5.1 Cases analyzed

Case	Specimen	Direction of horizontal load	Vertical load (t)	Remarks on loading conditions
1	WBW	Positive	25	One-way monotonic loading
2		Negative		
3		Positive	30	
4			20	
5	W-W	Positive	25	
6		Negative		
7		Positive	25	Pretension, 6 t, in connecting rods
8		Positive	30	One-way monotonic loading
9			20	
10	WWW	Positive	25	
11		Negative		
12	WBW-E	Positive	25	
13		Negative		
14	WBW-B	Positive	25	
15		Negative		
16		Positive	30	
17			20	
18		Positive	25	Cyclic loading
19		Negative		

6. CALCULATION PROCEDURE

Brick masonry walls of the five test specimens were not reinforced or lightly reinforced with horizontal steel bars. When analyzing the behavior of these structures subjected to horizontal loads, it is very difficult to get convenient solutions even if calculations are iterated for convergence, because the stress redistribution accompanied by the occurrence of cracking and slippage cannot be accomplished smoothly in the calculation. Therefore, in this paper, iterational calculations in order to get convenient solutions was not intended, but a small size of load or displacement increment in every step of calculation was used, thus leaving some amount of unbalanced forces over for the next step.

The calculation was performed after the tangent stiffness method. Loading sequences for the nineteen cases of calculations were as follows:

[Cases 1 to 6 and Cases 8 to 11]

Step 1	: Apply a vertical load of 25tf, 30tf or 20tf
Steps 2 to 16	. Apply horizontal load increments of 1.0tf up to a total horizontal load of 15tf
Steps 17 to 60	: Suppose a horizontal displacement increment up to a total horizontal displacement equal to 1.4 cm. If the load increment corresponding to the displacement increment exceeds 0.5tf, then a load increment of 0.5tf was adopted.

[Case 7]

Step 1	: Apply a total vertical loads of 25tf
Steps 2 to 7	: Apply the pretension with a 1-t increment
Steps 8 to 22	: Apply the horizontal load with an increment of 1.0tf up to 15tf
Steps 23 to 60	. Apply a horizontal displacement in steps up to 1.4 cm but so that the corresponding load increment did not exceed 0.5tf

[Cases 12 to 17]

Step 1	: Apply a vertical load of 25tf, 30tf or 20tf
Steps 2 to 16	: Apply the horizontal load with an increment of 1.0tf up to 15tf
Steps 17 to 100	: Apply a horizontal displacement in steps up to 4.0cm but so that the corresponding load increment did not exceed 0.5tf

[Cases 18 and 19]

Step 1	: Apply a vertical load of 25tf
Steps 2 to 16	: Apply positive horizontal load with an increment of 1.0tf up to 15tf
Steps 17 to 26	: Apply positive horizontal load with an increment of 0.5tf up to 20tf
Steps 27 to 66	: Apply positive horizontal load with a decrement of 0.5tf down to zero
Steps 67 to 81	: Apply negative horizontal load with an increment of 1.0tf up to 15tf
Steps 82 to 165	: Apply negative horizontal displacement in steps up to 4.0 cm but so that the corresponding load increment did not exceed 0.5tf

Calculation was stopped when the horizontal resistance of the specimen began to decrease. This was because results of calculation in an unstable specimen are not reliable

7. ANALYSIS RESULTS

7.1 Cases 1 to 4; Specimen WBW

In Fig. 7.1.1, horizontal load-horizontal displacement relations calculated in Cases 1 and 2 are compared with the corresponding hysteretic curve obtained in the test. It is observed that the calculated elastic rigidities were a little larger than the test results, but the ultimate shear strengths and the corresponding displacements are in good agreement with those observed in the experiment (see Table 7.1). In addition, the difference in the values of ultimate shear strengths for positive and negative loading is little. In this paper drift angle is defined as the ratio of horizontal displacement to specimen's height.

Table 7.1 Ultimate shear strengths and corresponding drift angles in Cases 1 to 4

Case	Ultimate Shear Strength			Drift Angle at Ultimate Strength	
	Test (tf)	Cal. (tf)	Test/Cal.	Test (10^{-3})	Cal. (10^{-3})
1	26.4	24.8	1.06	1.35	1.55
2	25.5	24.0	1.06	1.53	1.12
3	-	26.8	-	-	1.98
4	-	23.3	-	-	1.47

In Fig. 7.1.2, the load-displacement curves calculated in Cases 1, 3 and 4, in which vertical loads were 25tf, 30tf and 20tf, respectively, are compared. Effects of vertical load in the elastic region are not observed, but in the inelastic region where the horizontal load was higher than 17 or 18tf and inclined wall cracks had occurred. The effect of vertical load in this region is on the rigidity and ultimate shear strength: the higher is the vertical load, the larger are the rigidity and ultimate shear strength. Comparing Case 1 with Cases 3 and 4, it can be readily seen that an increase of vertical load by 20% caused an increase of ultimate shear strength of 8% and, also, that a 20% decrease of vertical load caused a 6% decrease of the ultimate shear strength. Comparable effects are observed in normal reinforced concrete columns and walls subjected to axial loads.

Calculated deformation patterns at a horizontal load of 18tf are shown in Figs 7.1.3 to 7.1.6 and are compared with test results. Calculated shapes are in good agreement with the test results. Note that displacement scales are different

Calculated crack development is shown in Figs 7.1.6 to 7.1.9 Crack patterns when horizontal loads reached ultimate shear strength are compared with those recorded in the experiments. Cracking evolution are similar in every case and can be described as follows:

1) Initial shear slips occurred along boundary surfaces between masonry walls and confining RC members.
2) Cracks occurred at lower corners of walls and continued along tie-columns and foundation beams.
3) During the extension of the cracks in lower positions of tie-columns, more shear cracking appeared in central parts of walls in the opposite side of the horizontal loading point. Similar shear cracks appeared, a little later, in another walls.
4) Shear cracks extended along the diagonal. Boundary surfaces between masonry walls and RC members separated. Maximum strengths were recorded for such condition.
5) Comparing Cases 2, 3 and 4, the higher the vertical load, the smaller the amount of inclined cracking in walls.

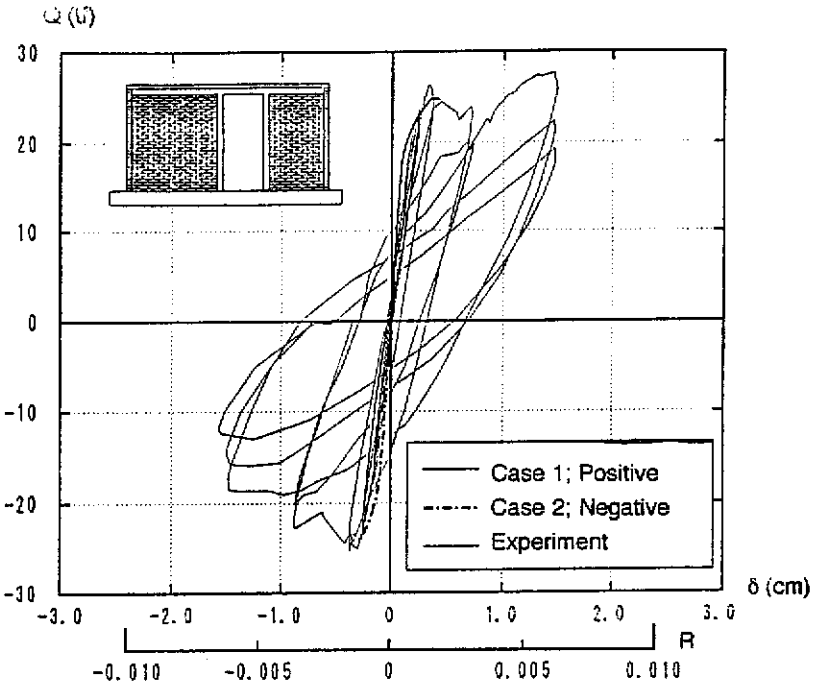

Fig. 7.1.1 Load (Q)-displacement (δ) relationships calculated in Case 1 and Case 2

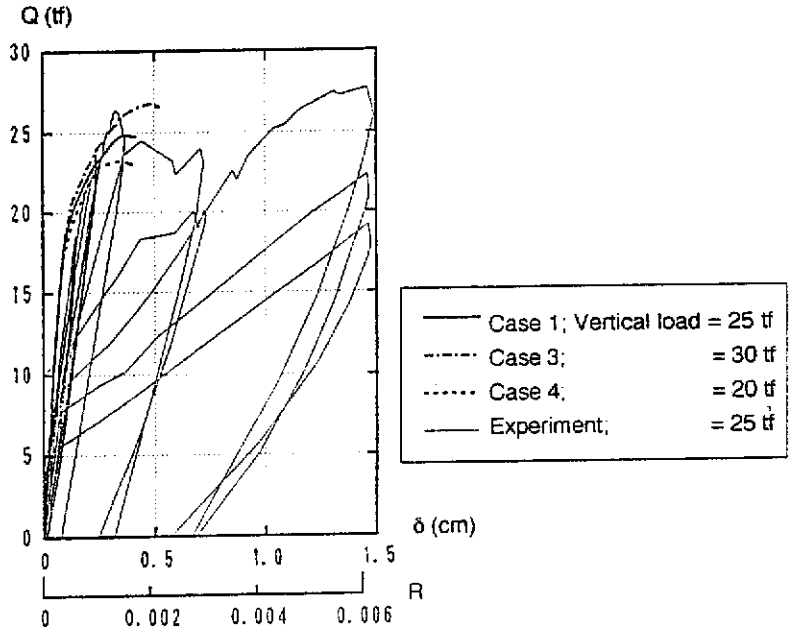

Fig. 7.1.2 Load (Q)-displacement (δ) relationships calculated in Case 1, Case 3 and Case 4

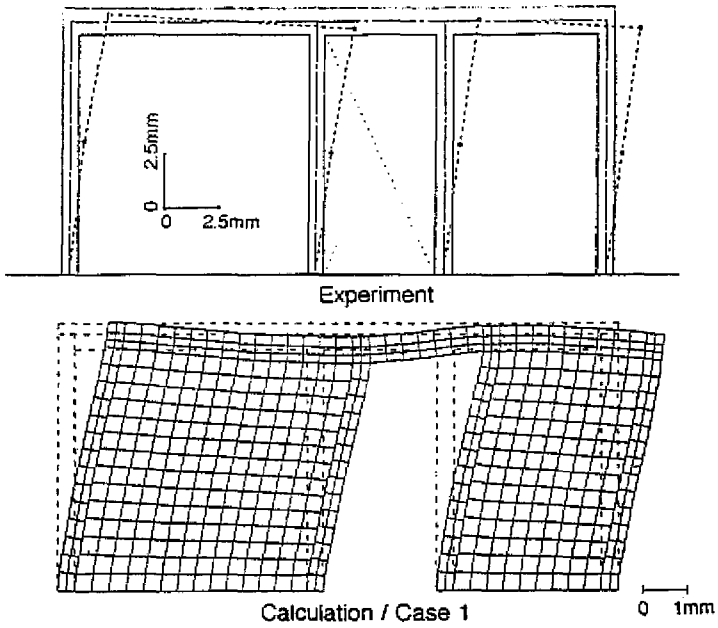

Fig. 7.1.3 Deformation pattern at a horizontal load of +18tf in Case 1 and its corresponding test result

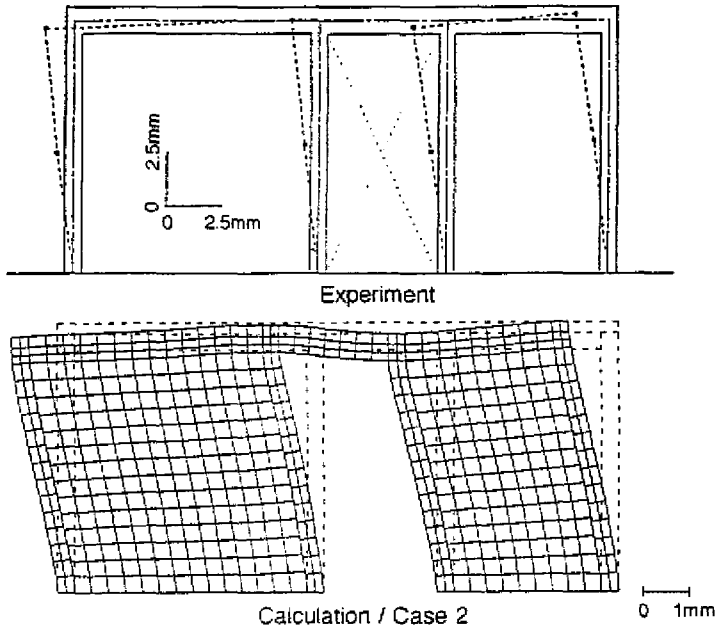

Fig. 7.1.4 Deformation pattern at a horizontal load of -18tf in Case 2 and its corresponding test result

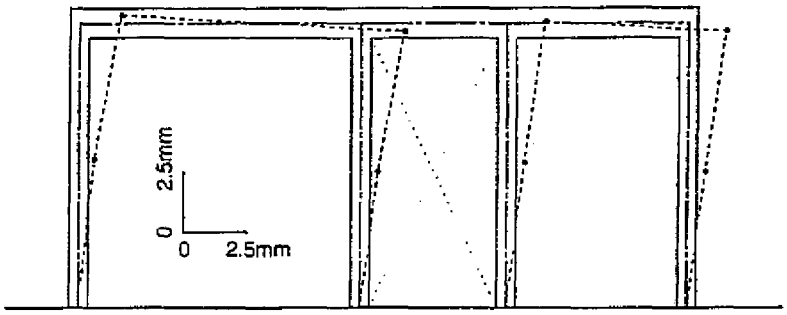

Experiment

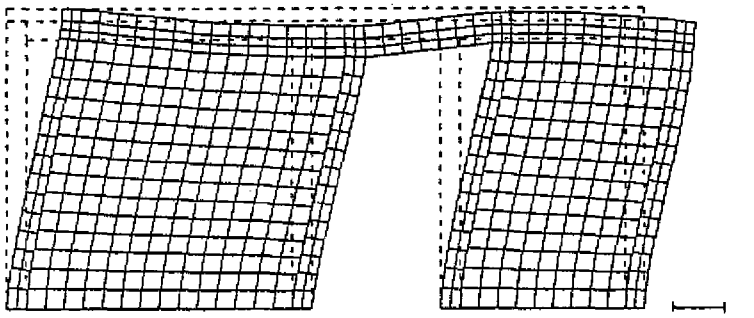

Calculation / Case 3

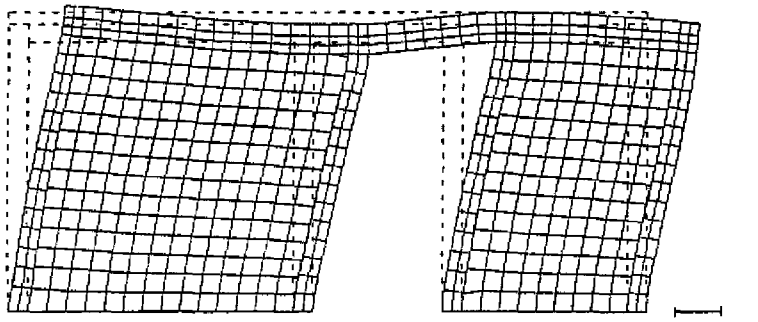

Calculation / Case 4

Fig. 7.1.5 Deformation pattern mode at a horizontal load of +18tf in Cases 3 and 4 and its corresponding test result

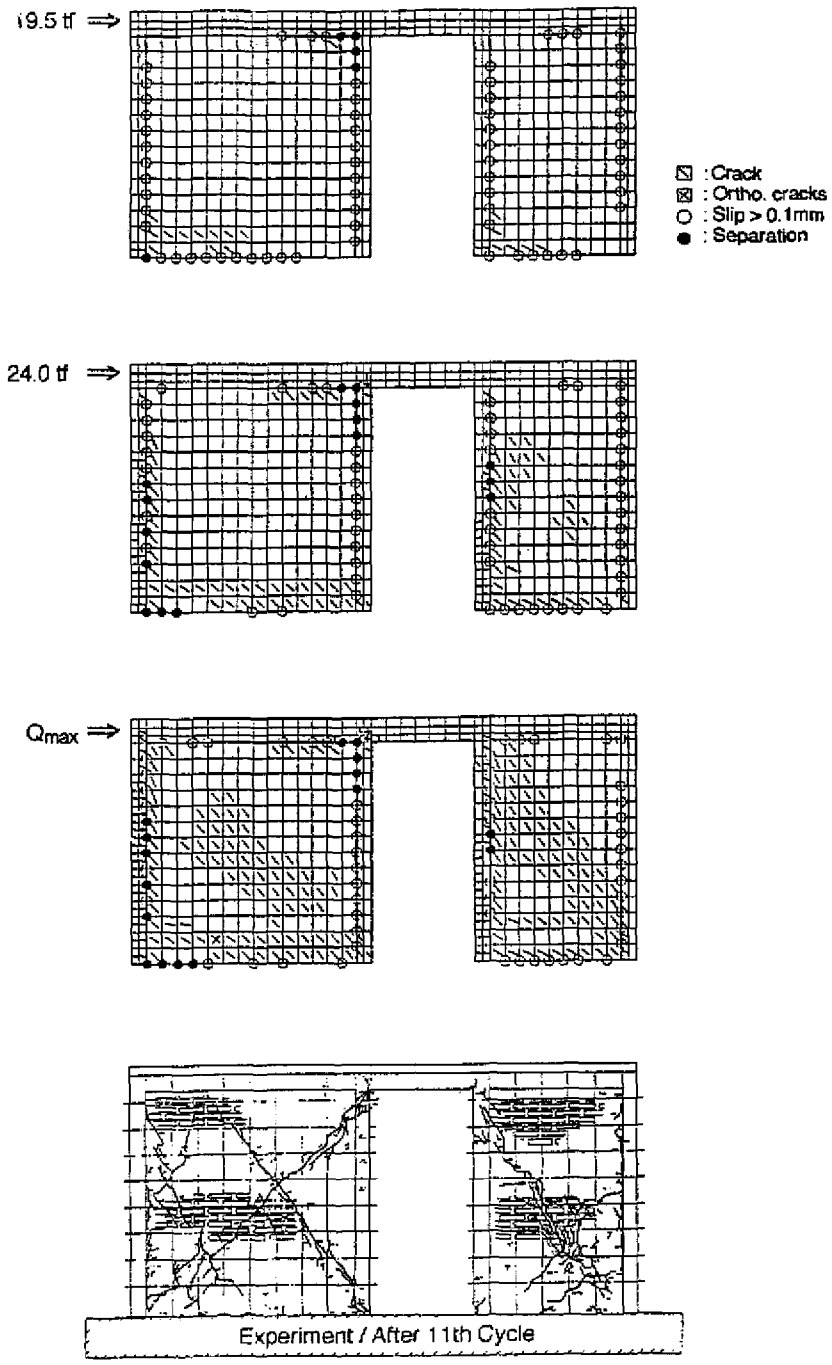

Fig. 7.1.6 Crack development in Case 1: WBW, positive loading, vertical load 25tf

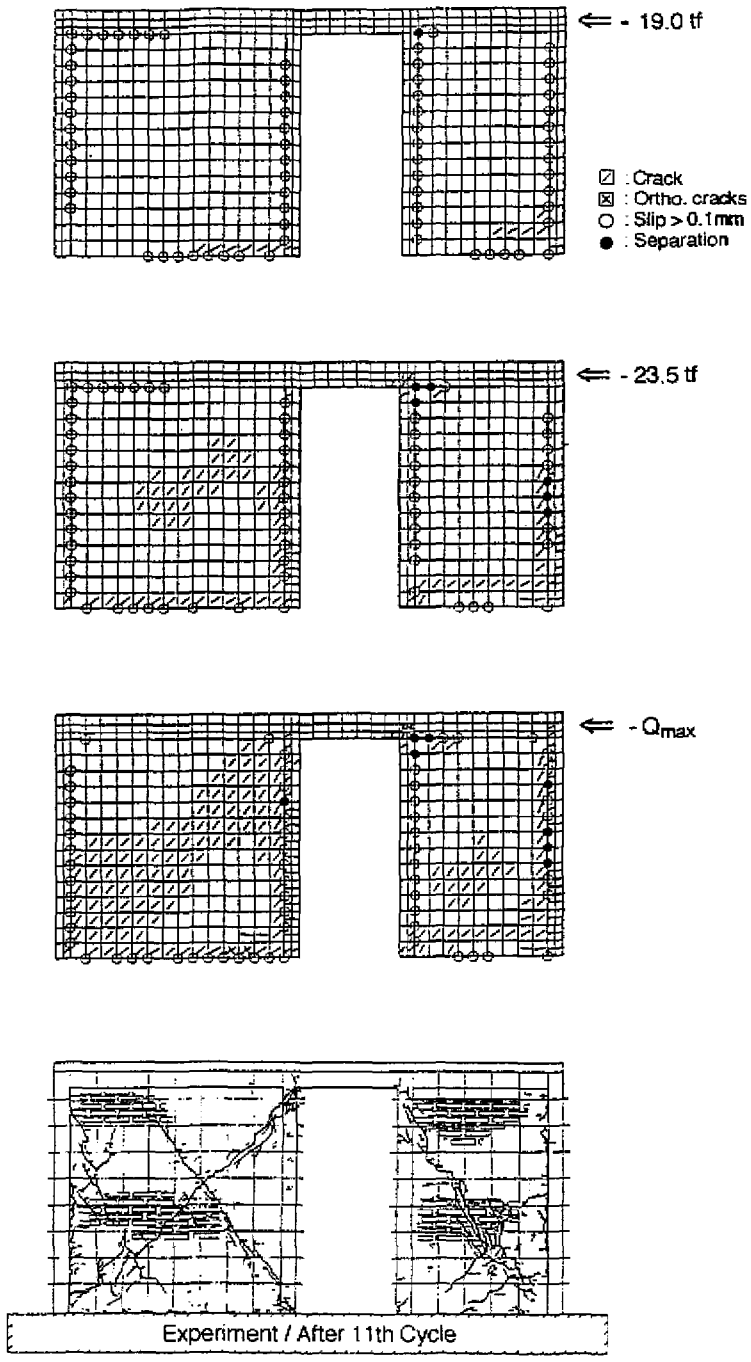

Fig. 7.1.7 Crack development in Case 2: WBW, negative loading, vertical load 25tf

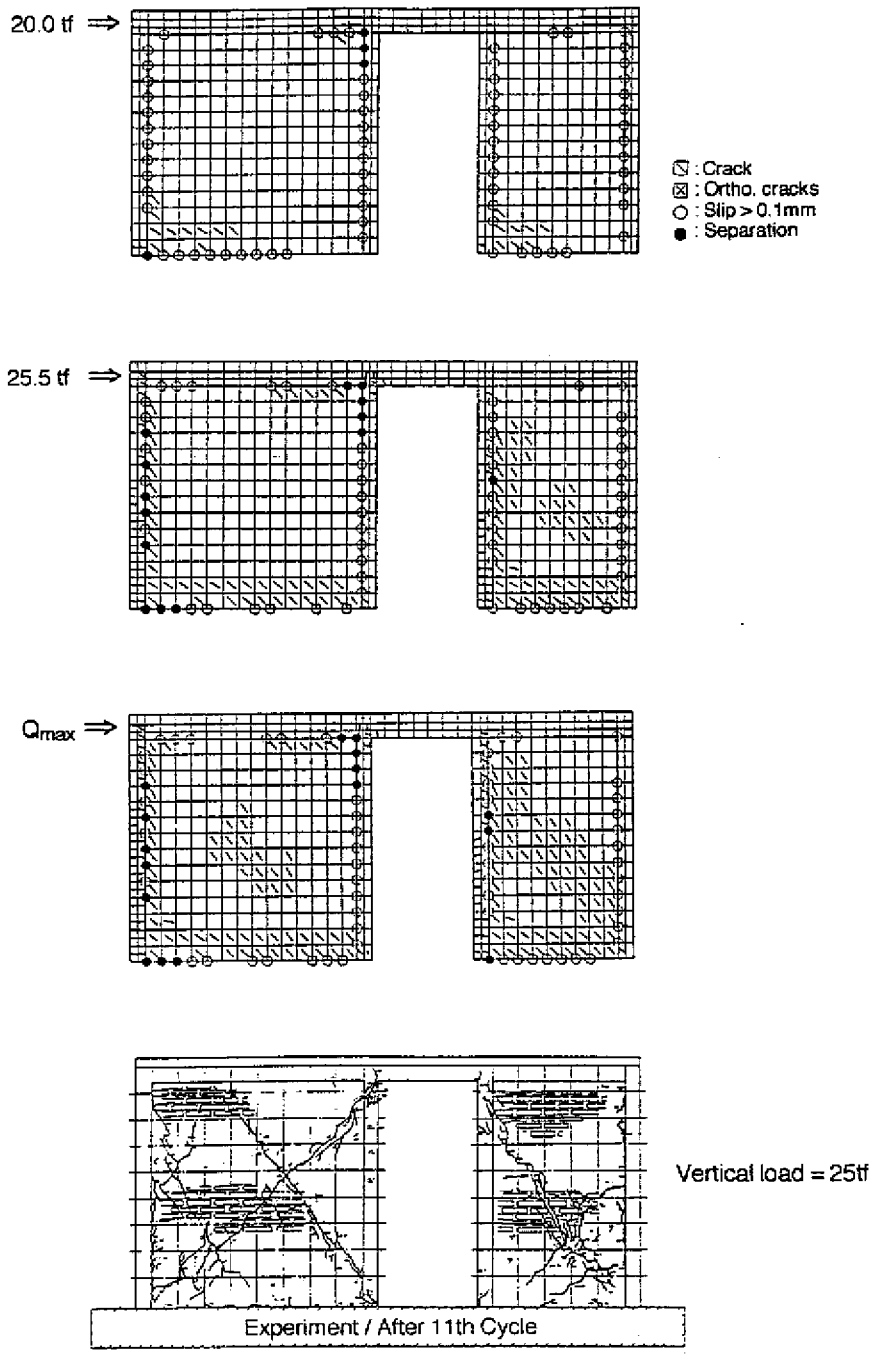

Fig. 7.1.8 Crack development in Case 3: WBW, positive loading, vertical load 30tf

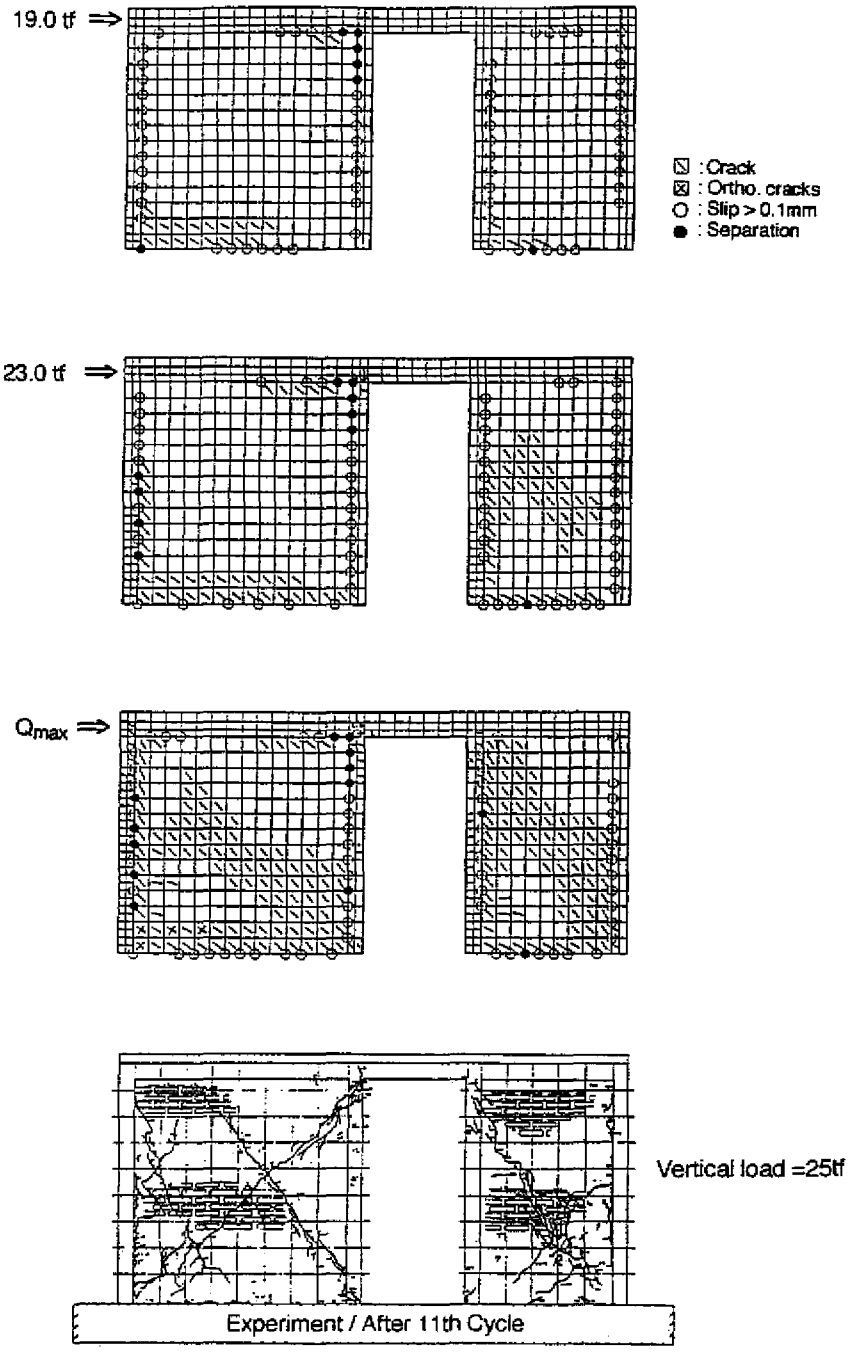

Fig. 7.1.9 Crack development in Case 4: WBW, positive loading, vertical load 20tf

7.2 Cases 5 to 9; Specimen W-W

In Fig. 7.2.1, horizontal load-horizontal displacement relations calculated in Cases 5 and 6 are compared with the corresponding hysteretic curves obtained in the experiments. It is observed in the figure that the elastic rigidity calculated in Case 5 was a little larger than the test result, but values of the ultimate shear strength and the corresponding displacement are in good agreement with test results (see Table 7.2). In Case 6, all those values are in good agreement with test results. In addition, due to effects of the loading sequence, the elastic rigidity was higher for positive loading, and the drift angle at the ultimate shear strength was larger for negative loading.

Table 7.2 Ultimate shear strengths and corresponding drift angles in Cases 1 to 4

Case	Ultimate Shear Strength			Drift Angle at Ultimate Strength	
	Test (tf)	Cal. (tf)	Test/Cal.	Test (10^{-3})	Cal. (10^{-3})
5	22.2	23.2	0.96	1.38	1.33
6	24.0	23.1	1.04	1.57	1.54
7	22.2	23.0	0.97	1.38	1.29
8	-	23 7	-	-	1.23
9	-	21.8	-	-	1.40

In Fig. 7.2.2, the load-displacement relation calculated in Case 7 is compared with that obtained in Case 5. No difference was observed between those two relations so that the pretension, which was recorded in the test and analytically introduced in the connecting rods, had no effect on the seismic behavior of specimen W-W.

In Fig. 7.2.3, the load-displacement relations in Cases 5, 8 and 9 are compared to discuss the effect of the vertical load. From this figure and Table 7.2, similar effects of vertical load as those described in the preceding section (7.1) can be observed.

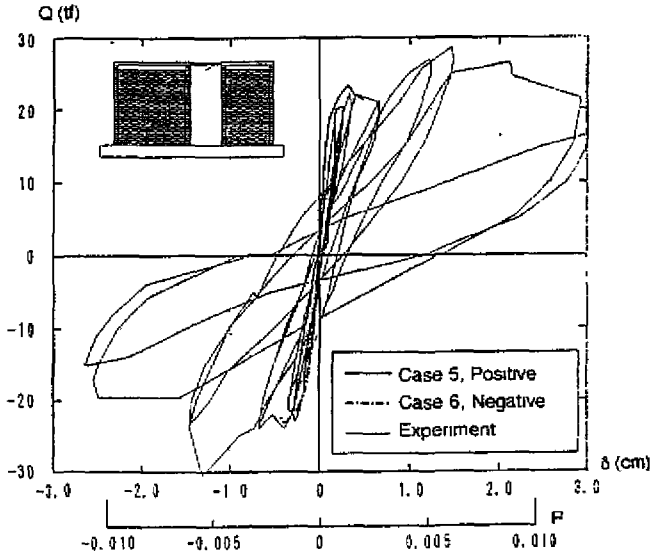

Fig. 7.2.1 Load (Q)-displacement (δ) relationships calculated in Case 5 and Case 6

Calculated deformation patterns at a horizontal load of 18tf are shown in Figs 7.2.4 to 7.2.9 and are compared with test results. Calculated patterns are in good agreement with test results.

Computed crack development is shown in Figs 7.2.10 to 7.2.14. Crack patterns for horizontal loads corresponding to the ultimate shear strength are compared with those recorded in the tests. In these graphs, it can be observed that inclined cracks appeared on many finite elements along the diagonals of brick walls in every case.

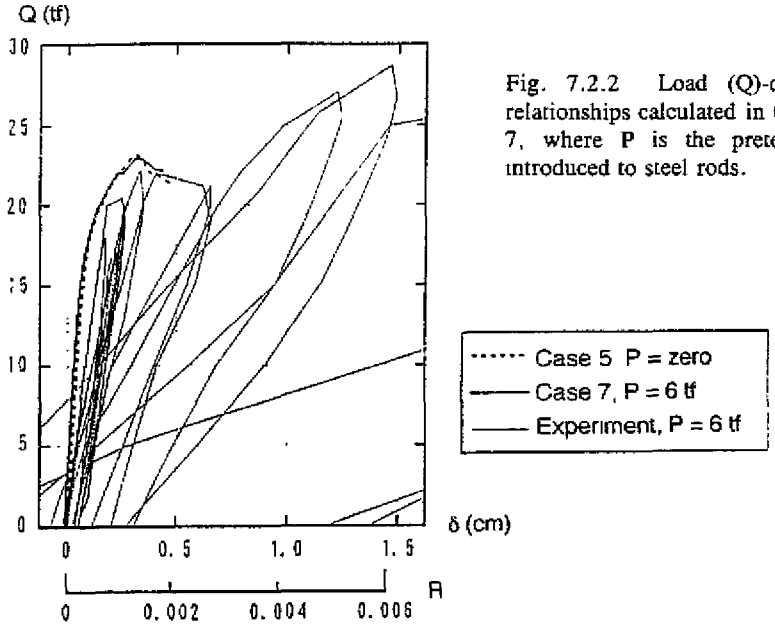

Fig. 7.2.2 Load (Q)-displacement (δ) relationships calculated in Case 5 and Case 7, where P is the pretension which is introduced to steel rods.

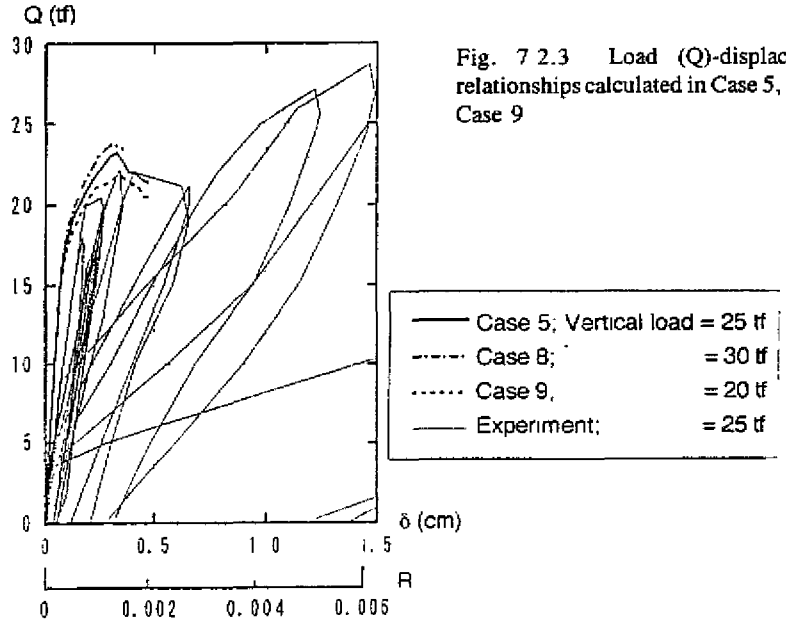

Fig. 7.2.3 Load (Q)-displacement (δ) relationships calculated in Case 5, Case 8 and Case 9

In the experiments, however, the number of diagonal cracks in brick walls was not so many but a few cracks were predominant. In spite of this difference, we can conclude that the crack patterns obtained by calculations may suggest a good image of the real phenomenon.

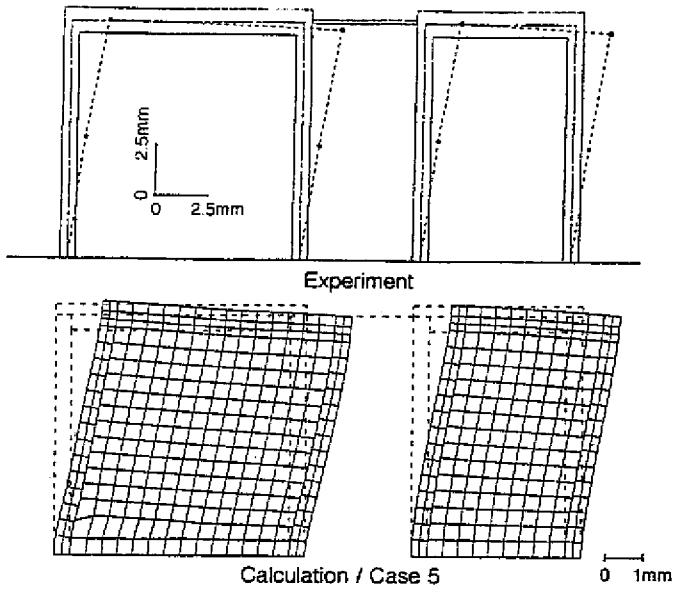

Fig. 7.2.4 Deformation pattern at a horizontal load of +18tf in Case 5 and its corresponding test result

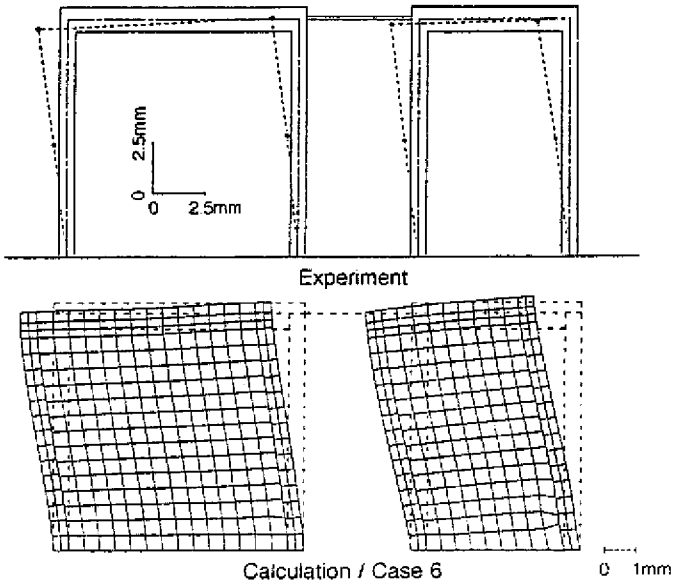

Fig. 7.2.5 Deformation pattern at a horizontal load of -18tf in Case 6 and its corresponding test result

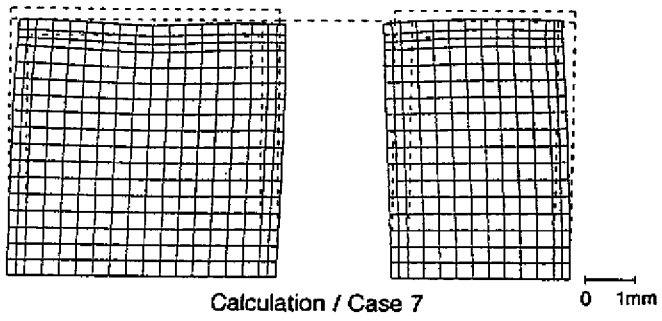

Fig. 7.2.6 Deformation pattern when 6tf pretension was analytically introduced to the connecting rods of Specimen W-W

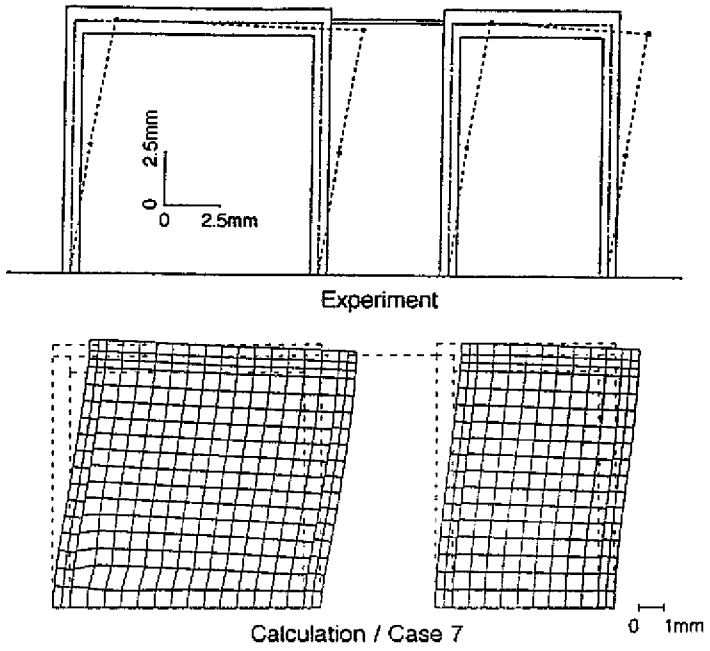

Fig. 7.2.7 Deformation pattern at a horizontal load of +18tf in Case 7 and its corresponding test result

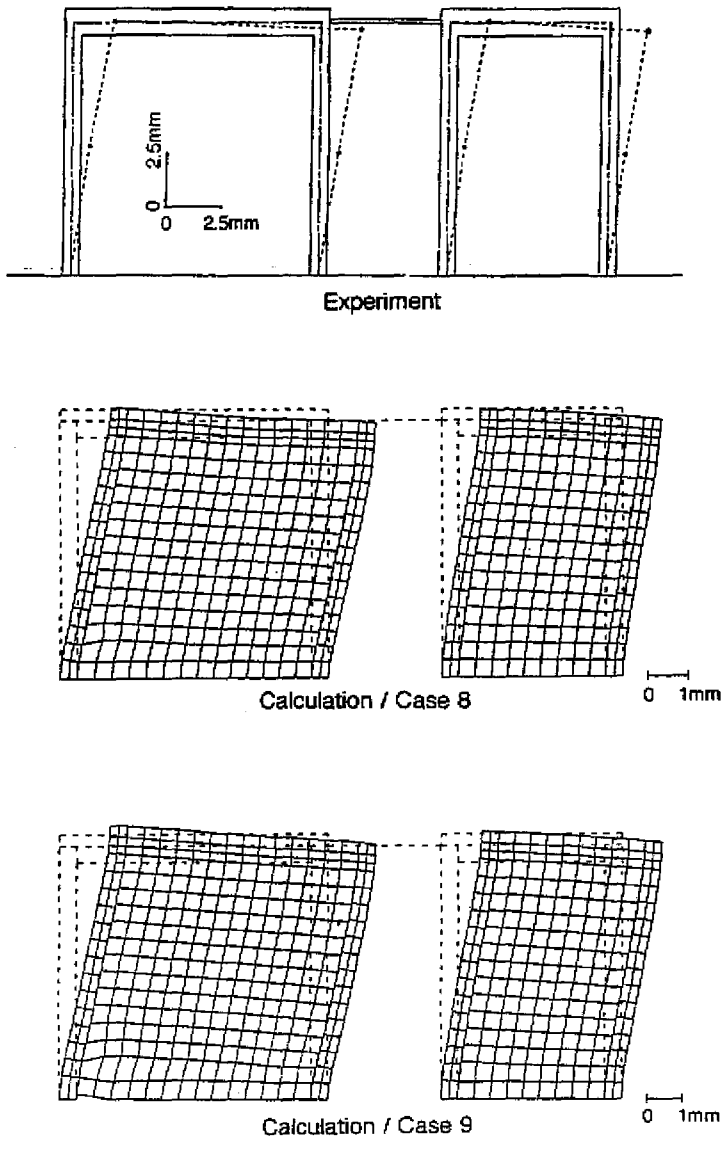

Fig. 7.2.8 Deformation pattern at a horizontal load of +18tf in Case 8 and Case 9 and its corresponding test result

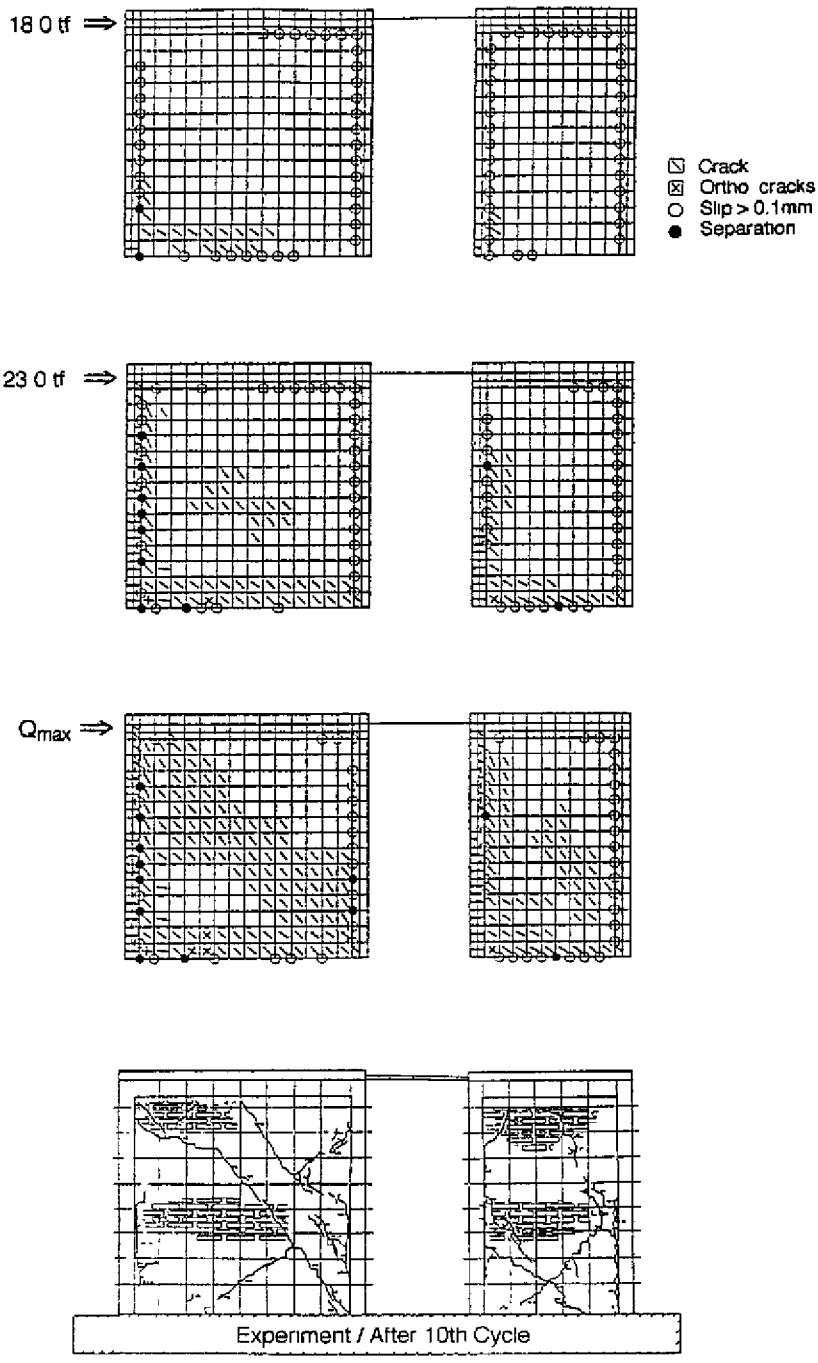

Fig 7.2.9 Crack development in Case 5: W-W, positive loading, standard axial load (25 t)

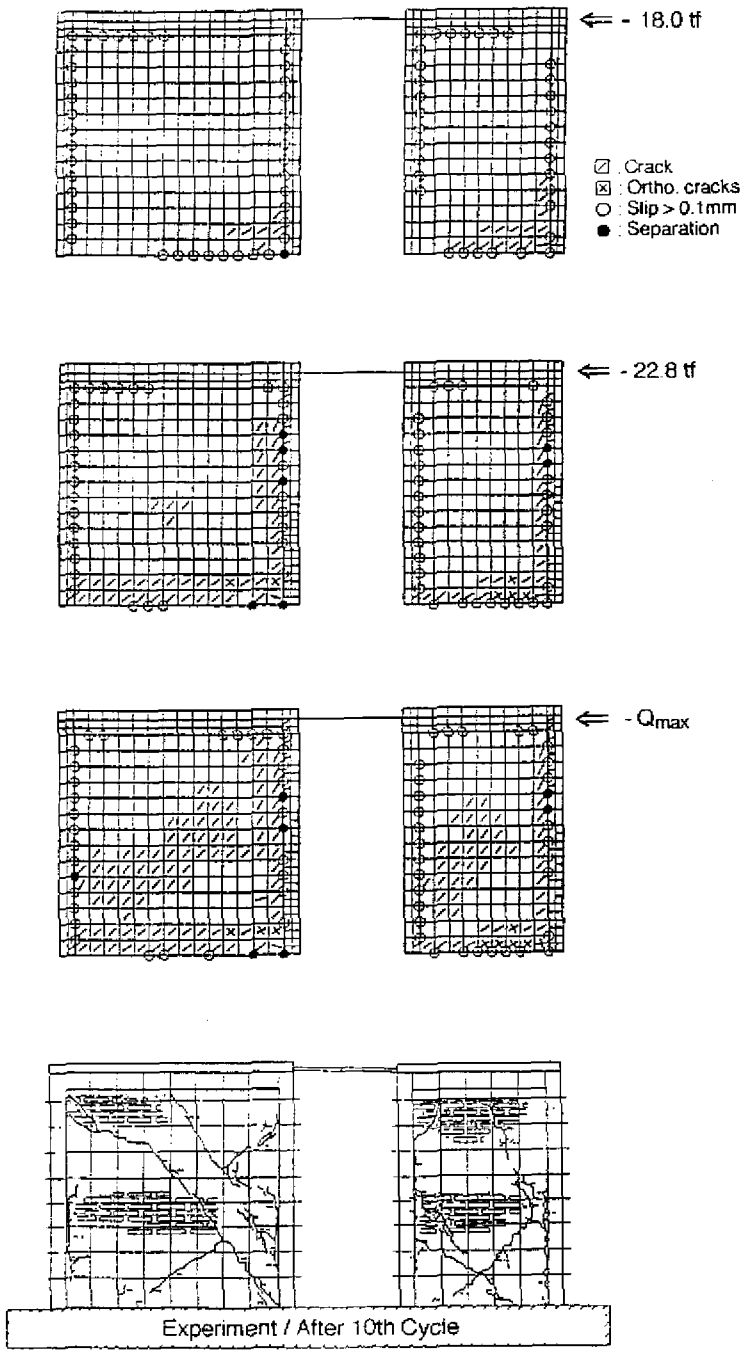

Fig. 7.2.10 Crack development in Case 6: W-W, negative loading, standard axial load (25 t)